USE OF SMALL-ANGLE NEUTRON SCATTERING FOR THE CHARACTERIZATION OF ANISOTROPIC STRUCTURES PRODUCED BY THERMAL SPRAYING

JAN ILAVSKY*, **, GABRIELLE G. LONG**, ANDREW J. ALLEN**, HERBERT HERMAN***, CHRISTOPHER C. BERNDT***

*Institute of Plasma Physics, Academy of Sciences of the Czech Republic,
Za Slovankou 3, 182 00 Prague
E-mail: ilavsky@ipp.cas.cz

**National Institute of Standards and Technology,
Gaithersburg, MD 20899, U.S.A.

***State University of New York at Stony Brook,
Stony Brook, NY 11973, U.S.A.

Received November 11, 1997.

Results for the microstructural characterization of thermal spray deposits, using small-angle neutron scattering (SANS), mercury-intrusion porosimetry, and image analysis of polished cross sections, are compared. The alumina and yttria-stabilized zirconia deposits studied were produced by two different atmospheric plasma-spraying methods - using gas-stabilized and water-stabilized plasma systems. The void microstructure of these deposits is dominated by two anisotropic void types - interlamellar pores and intralamellar cracks. There is also a broad distribution of spherical pores. The relative importance of these void systems is found to depend on the materials chemistry and on the spray technique. The surface area of the anisotropic voids was determined using SANS. By varying the spray technique and material, deposits with different dominant void systems were produced. The alumina deposits, manufactured by a high-power water-stabilized plasma-spray system, consisted of a microstructure dominated by intralamellar cracks; the same material deposited by a standard lower-power gas-stabilized plasma-spray system has about equal surface area in the intralamellar cracks and interlamellar voids. However, the zirconia deposit microstructure is always dominated by inerlamellar voids.

INTRODUCTION

Thermal spraying is a well known method for producing a wide range of deposits on a variety of surfaces and for producing free-standing parts. Substrates which may be coated range from metals, through intermetallics, the ceramics and plastics. The materials which can be deposited cover almost as wide a range. The major limitation on both substrate and deposition material is the requirement that it does not decompose during the spray process [1].

During thermal spraying the deposited material (feedstock) is heated (normally to the melt) and accelerated toward the substrate [2, 3] such that a stream of molten or semi-molten particles impacts on the substrate. Each particle on impact spreads and creates a basic building block of the thermal deposits - the splat or lamella. The process of splat formation and cooling is a rapid solidification process with cooling rates of around 10^4 K s^{-1} and 10^5 K s^{-1} [1].

The deposits are often composed of metastable phases [4, 5]. After deposition and subsequent cooling stresses are often built up within the splats, where this may cause cracking or sliding of splats. Further stress formation may occur when deposit/substrate system cools to room temperature due to different coefficient of thermal expansion. During product application, its environment can cause phase changes, stress formation or relaxation and other irreversible changes in the substrate/deposit system [6, 7].

The void structure of the thermally-deposited ceramic materials represents an unusual void structure dominated by anisotropic interlamellar pores and intralamellar cracks, and may include a broad distribution of rounded voids [8]. The pores and cracks have different anisotropy with one common isotropic direction, usually the deposition direction. The interlamellar pores are mostly parallel with the substrate whereas the intralamellar cracks are mostly perpendicular to the substrate [9, 10, 11]. In this work applied small-angle neutron scattering (SANS) technique takes advantage of this anisotropy [12, 13]. The description of the isotropic rounded voids is beyond the scope of this paper.

This work describes novel technique for the characterization of anisotropic microstructure and compares it with results which can be obtained by standard techniques (mercury intrusion porosimetry and image analysis).

EXPERIMENTAL PART

Small-angle neutron scattering

Small-angle neutron scattering can be particularly useful for studying the processing-microstructure relationships of ceramic materials [14, 15]. The total specific surface area of the voids can be derived from the terminal slope in SANS spectra, i.e., Porod scattering [16]. Porod scattering measurements enable a direct determination of the surface areas of both the open and the closed voids in a material, independent of the void morphology.

A schematic of the SANS experiment is shown in figure 1. A monochromated and collimated beam of cold neutrons, with wavelength selected by the velocity selector, passes through the sample.

These neutrons are scattered within the sample and are measured on a two-dimensional detector.

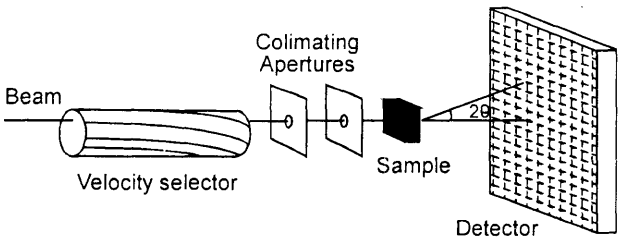

Figure 1. Schematics of the small angle neutron experiment.

The voids and the grains within the samples have different scattering length density, ρ, causing some of the neutrons to be scattered at the void/grain interfaces. The scattered intensity, I, is a function of the scattering wave vector **Q**, where $|\mathbf{Q}| = (4\pi/\lambda)\sin(\theta)$, and 2θ is the scattering angle [17]. I(**Q**) depends on the volume fraction, ϕ, of porosity, on the scattering contrast (which is the square of the difference in scattering length densities between the grains and the voids, $(\Delta\rho)^2$), and on the distribution of void sizes. When the microstructure of a scattering sample is isotropic, the scattered intensity depends simply on $Q = |\mathbf{Q}|$, rather than on **Q**.

In the dilute limit where there are very few scatterers, only a small fraction of the incident neutrons are small-angle scattered and a SANS analysis assuming single-scattering (Guinier and Porod) and diffraction theory is used. The scattered profile as a function of **Q** can be used to derive information on the shape, size distribution, volume fraction and surface areas of the scattering features even for anisotropic microstructures, provided that the scattered intensity is averaged over all orientations of **Q**. For a particular **Q**, the information refers to dimensions parallel to **Q** [16, 17]. For copious numbers of scattering voids in the 0.1 μm to 10 μm size range, as is observed in plasma-sprayed ceramics, a multiple-scattering formulation (MSANS) can be employed [18] to extract many of the same microstructural parameters available in a Guinier analysis. In this paper, however, we limit the discussion to an analysis of the data in the single-scattering Porod regime, which is observed at large **Q** even in the presence of multiple scattering [12, 19] at low **Q**.

The Porod scattering regime [16, 17] extends over the region in the data for which $QL > 3$, where L is the smallest dimension in the scatterers. For isotropically-distributed microstructures, the scattering cross section $d\Sigma/d\Omega$ (which is proportional to the scattered intensity) is given by the Porod scattering relationship:

$$\frac{d\Sigma(Q)}{d\Omega} = \frac{2\pi(\Delta\rho)^2 S_V}{Q^4} \quad , \tag{1}$$

where S_V is the total specific surface scattering area of the voids. Since the material is a two phase (grains + voids) system, where the scattering occurs at the boundaries between solid and void, S_V is the total pore/solid and crack/solid surface area per unit sample volume. To obtain a complete description of the void system, the values for S_V need to be used together with information on the sizes, volumes and shapes of the voids. Such a description will follow in a subsequent paper [20].

Electron microscopy results (figures 2 and 3) have shown that the voids in plasma-sprayed ceramics are polydisperse in both size and shape. Furthermore, the voids are preferentially oriented. However, the microstructure viewed from top (in the substrate plane) is isotropic [12]. This is important, because the presence of one circularly-symmetric direction (perpendicular to the substrate) in the plasma-sprayed microstructure is key to enabling a quantitative three-dimensional analysis of the microstructure from the scattering data.

To derive the total surface area of voids within an anisotropic material, the scattered intensity can be measured and averaged for all sample-beam orientations, covering all possible angles. For plasma-sprayed samples, this procedure would not necessarily distinguish among the distinct structures in the deposit. Instead, we have measured the scattering along selected directions of **Q**, enabling us to derive separately the parameters of the individual void structures, which contribute to the anisotropic scattering patterns.

For monodisperse spheroids (ellipsoids of revolution) with orthogonal radii R, R, and βR, the anisotropic Porod

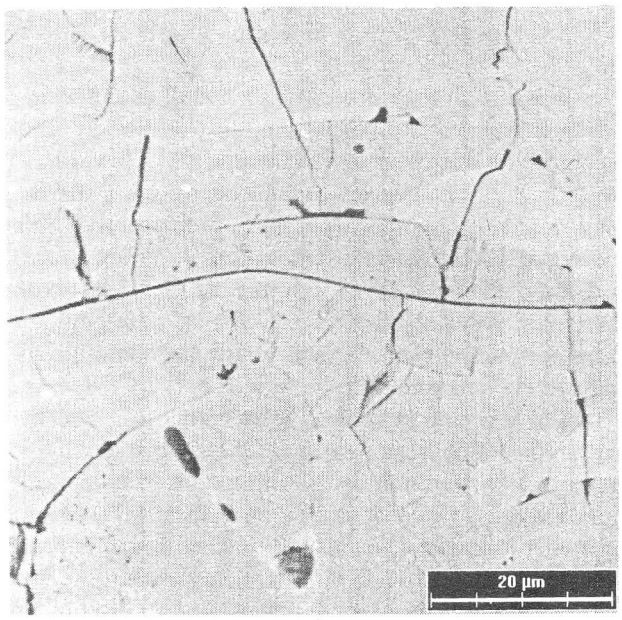

a)

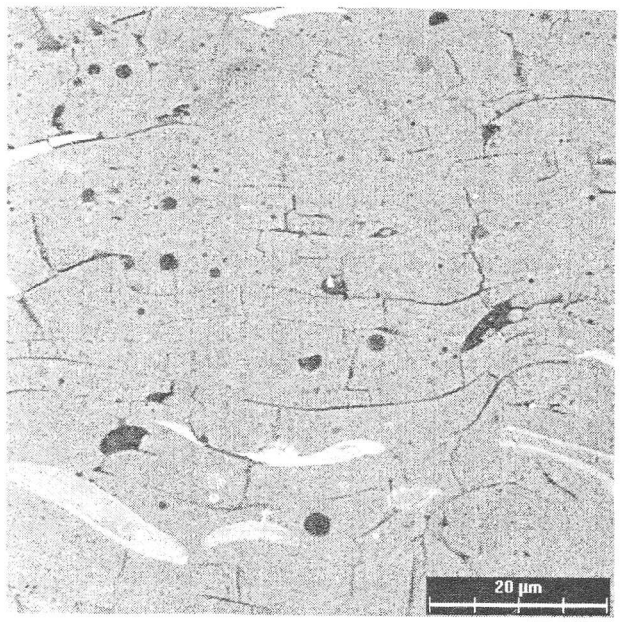

b)

Figure 2. Micrographs of *a)* WSP® alumina and *b)* GSP alumina. The SEM mode was BE.

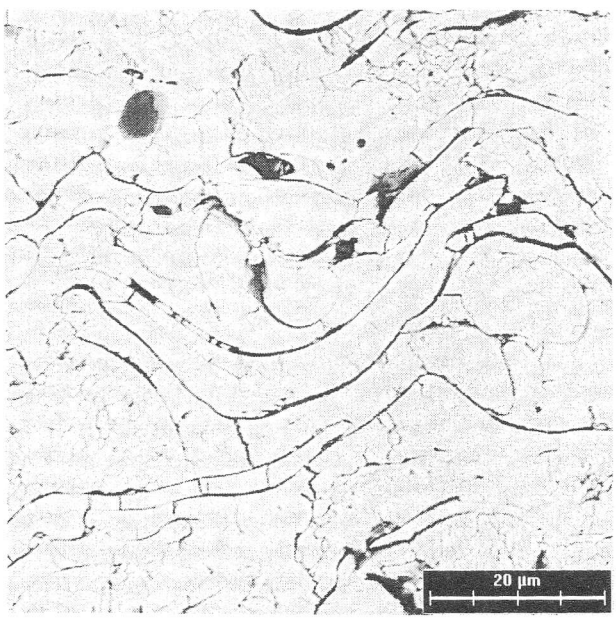

a)

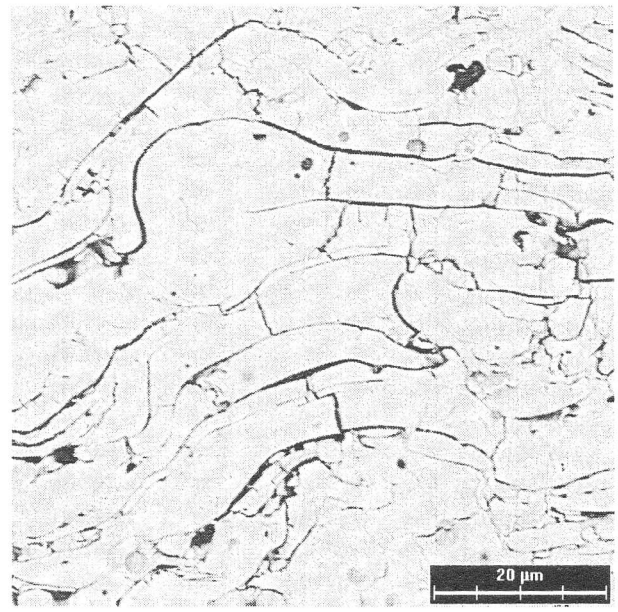

b)

Figure 3. Micrographs of *a)* WSP® CaSZ and *b)* GSP YSZ. The SEM mode was BE.

scattering can be calculated analytically. Following the analysis of Hamzeh and Bragg [19] equation 1 becomes:

$$\frac{d\Sigma(\vec{Q})}{d\Omega} = \frac{2\pi|\Delta\rho|^2}{Q^4} \quad \frac{3\phi}{R} \quad \frac{\beta}{[1+(\beta^2-1)X^2]^2} \quad , \qquad (2)$$

where ϕ is the volume fraction of the spheroidal voids and $X = \cos\eta$, where η is the angle between Q and the βR axis of spheroidal symmetry. ($X = 0$ when **Q** is perpendicular to the βR axis and $X = 1$ when **Q** is parallel to the βR axis.) Note that for spheres (i.e., $\beta = 1$) Equation 2 reduces to equation 1 since $S_V = 3\phi / R$.

The anisotropy in the Porod scattering, given by equation 2, is strongly amplified with the shape of the scatterers. While the anisotropy in the scattering is not strictly spheroidal itself, even mildly oblate spheroidal scatterers, of fixed orientation, will give markedly prolate anisotropic Porod scattering. Similarly, mildly prolate scatterers, of fixed orientation, will give markedly oblate Porod scattering.

In practice, the anisotropy in the Porod scattering depends not only on the individual pore shapes and preferred orientation, but also on the polydispersity of pore shapes and sizes, and to some extent on the surface roughness. High surface roughness, and considerable polydispersity in pore shapes and sizes, would give anisotropic Porod scattering that is linearly proportional to the interfacial surface area projection in the plane perpendicular to **Q** [16, 17]. Even for monodisperse spheroids, equation 2 must be averaged over the orientational distribution. For random orientations, the anisotropy disappears and equation 1 is recovered. However, in the present case of two dominating and coexisting pore/crack morphologies with different preferred orientations and sizes and with relatively smooth interfacial surfaces and geometric symmetries (e.g., oblate spheroidal cracks with parallel sides), equation 2 is illustrative of the coexisting strong anisotropies that may be observable in the Porod scattering by plasma-sprayed deposits. Spherical voids, also present in the microstructure (figures 2 and 3) do not add significantly to Porod surface area (large pores with small surface area) and cannot be distinguished by this technique.

It should be noted that particular preferred orientational distributions of the scatterers may be masked in the anisotropy of the Porod scattering. For example, a two-dimensional random orientational distribution of oblate scatterers, all with a short βR axis approximately in one plane, would give rise to Porod scattering that is also oblate in its anisotropy, with the axis of symmetry and the direction of least Porod scattering perpendicular to the orientational averaging plane.

If the Porod scattering can be measured for all orientations of **Q** over 4π solid angle, none of the above uncertainties in pore shape or morphology prevents a determination of the total interfacial surface area per unit sample volume, $S_{V\ TOTAL}$. By averaging $d\Sigma(\mathbf{Q})/d\Omega$ over all orientations of **Q**, we obtain:

$$\left\langle \frac{d\Sigma}{d\Omega} \right\rangle_{ORIENTATION} = \frac{2\pi|\Delta\rho|^2 S_{V\ TOTAL}}{Q^4} \quad , \qquad (3)$$

where $\langle \cdots \rangle$ implies an orientational average.

Equation 3 reduces to equation 1 in the case of random orientations or an isotropic microstructure. When different coexisting pore morphologies can be discerned from the orientational variation of $d\Sigma(\mathbf{Q})/d\Omega$, these anisotropic components can be orientationally averaged separately. Thus, $S_{V\ TOTAL(i)}$ can be determined for the i^{th} pore/crack morphology in the system.

Image analysis

Image analysis of the cross section of mounted and polished samples is probably the most commonly used technique for microstructure evaluation [21]. However, in the case of plasma-sprayed ceramic deposits it is also the least reproducible one. The main problem with this technique is the sample preparation - grinding and polishing. Plasma-sprayed ceramic deposits are weak structures which regularly break during polishing and therefore pull-outs are formed. These may significantly obscure the structure [22].

Various improvements were proposed for the preparation of polished surfaces of these weak structures; impregnation with thin epoxy, infiltration of pores with other materials (for example Cu from chemical solution) and other methods were applied. None of these normally valuable techniques offers convincing reliability and reproducibility [23].

Careful polishing combined with cautious evaluation of images offers most valuable insight in the voids shapes and orientations. The volumes of voids measured by this technique may, however, be significantly distorted by the presence of pull outs, anisotropy of the sample and possibly low resolution limit.

Mercury intrusion porosimetry

Mercury intrusion porosimetry (MIP) is probably the second most commonly used technique for porosity characterization of plasma-sprayed deposits [24]. It is based on the intrusion of mercury into the pores of a sample as a function of pressure. The radius, r, of a void that is filled at a given pressure is given by Washburn's equation [25, 26]:

$$P_h = -(2\gamma/r)\cos\theta \quad , \qquad (4)$$

where P_h is the mercury pressure, γ is the surface tension of mercury (480×10^{-3} N m^{-1}) and θ is the wetting or contact angle (which for most materials is close to 140° [25]). Void diameters from about 100 μm, at pressures below atmospheric pressure, to about 3 nm, at pressures of approximately 22.8 MPa, can be measured [26]. A variation of the MIP technique is the so-called Archimedes method, in which the sample is infiltrated by water at atmospheric pressure and densities are calculated from the difference in the weight of the sample dry and soaked [27].

Both techniques allow a calculation of the volume of open porosity and also the residual density. If the skeletal density is known, than the volume of closed porosity can be calculated. The Washburn's equation in the form presented here uses the cylindrical-pore-shape model which is the most used model. The generalization to

other shapes may also be done [24]. While the densities and therefore the volumes of porosities derived from both of these techniques are quite reliable, the pore size distributions from MIP are less useful. The presence of small necks between relatively large pores may shift the calculated curve to smaller pore sizes. Complex and irregular pore shapes may have also significant influence.

EXPERIMENT

Samples were deposited by the atmospheric plasma spraying method. In this case the spraying is done at ambient pressure and atmosphere, compared to low or high pressure plasma spraying, when the atmosphere is controlled and pressures are lower or higher than ambient, respectively. The plasma torch contains a cathode and an anode between which there is a burning electric arc. This arc is stabilized by a plasma-forming medium, usually gas or less usually water vapors. In our case two plasma spray systems were used - the more usual gas-stabilized plasma system, manufactured by Plasma-Technik*, Switzerland, and water-stabilized, manufactured by Institute of Plasma Physics*, Czech Republic. The standard gas-stabilized system has lower power (about 40 kW) compared with water-stabilized system (about 160 kW). The water-stabilized system also produces higher temperatures in the flame, and since the operating power is higher and water vapor has a higher enthalpy compared with standard plasma forming gases, it allows higher throughput.

Water-stabilized plasma (WSP®) spray system (PAL160*) and gas-stabilized plasma (GSP) spray system (Plasma Technik F4*) at the Thermal Spray Laboratory, State University of New York at Stony Brook were used to prepare the samples. The WSP® system was operated at about 160 kW input (320 V, 500 A) with about 35 kg h^{-1} (about 583 g min^{-1}) of alumina and 49.7 kg h^{-1} (about 828 g min^{-1}) of zirconia feedstock fed through two injectors. The feeding distance was 30 mm, the spray distance was 350 mm for alumina and 260 mm for zirconia. For the GSP system the spray nozzle diameter was 8 mm, the powder injector diameter was 1.8 mm, and the current was 500 A at 68 V. The primary gas was argon (40 l min^{-1}), the secondary gas was hydrogen (10 l min^{-1}), and the carrier gas was argon (3 l min^{-1}). The powder feed rate was 26 g min^{-1}. The spray distance was 90 mm for zirconia feedstock and 100 mm for alumina feedstock.

Alumina and zirconia were studied. Both are rarely used in their pure form for plasma spraying. Alumina is usually doped with 3% to 40% (all percentages in this paper are mass fractions) of TiO_2 and zirconia is usually doped with about 8% Y_2O_3 or 5% CaO. The doping material present is in each material for different reason - in alumina it increases the toughness whereas in zirconia it is present to stabilize the mid-range temperature tetragonal phase to room temperature. The parameters for the feedstock are given in table 1.

Table 1. Parameters of the feedstock materials.

manufacturer/ /material	composition (wt.%)	size range** $d10$, $d90$ (μm)	spray method
Alloy Metals, Inc. Amdry 142*	ZrO_2, 8 Y_2O_3	41, 113	GSP
Norton 235*	ZrO_2 + 5.1 CaO, 0.1 MgO, 0.1 SiO_2, 0.4 Al_2O_3, 0.1 Fe_2O_3, 0.2 TiO_2, 0.1 other oxides	45, 75	WSP®
Norton Gray alumina*	Al_2O_3 + 2.7 TiO_2, 0.8 SiO_2, 0.1 Fe_2O_3, and 0.6 other oxides	46, 124	WSP®
Metco 101B-NS*	Al_2O_3 + 2.5 TiO_2, 2 SiO_2, 1 Fe_2O_3 and 0.5 of other oxides	40, 116	GSP

** 10 % of the diameters are smaller than d_{10}, and 90 % of the diameters are smaller than d_{90}.

To obtain free-standing deposits, approximate 5-mm--thick deposits were sprayed onto a mild steel substrate (50 mm × 25 mm × 2.5 mm) that had previously been covered with an Al layer (deposited by wire-arc spraying). After spraying, the Al layer was desolved to obtain free-standing deposits. A low speed diamond saw was used for sectioning the samples to about 25 mm x × 5 mm x 5-mm thick. Samples were further cut into smaller pieces where necessary.

For MIP, 1 g to 2 g of each sample were cut into pieces small enough to fit in the small sample cell (0.5 cm^3) of a commercially-available MIP system (Autoscan 33*, Quantachrome Corp., FL). The system was supplied with software programs for data collection and analysis. Conventional parameter values such as a constant contact angle $\theta = 140°$, constant surface tension $\gamma = 0.480$ N m^{-1}, were used. No corrections for sample compressibility and mercury compressibility were made. The corrections for an empty run and other factors were not carried out as these are built into the system. Pressure and intruded volume data were recorded in the range of 0.01 MPa to 22.8 MPa, corresponding to pore sizes between 100 μm and 3 nm in diameter.

Samples cut in the cross section were mounted in polyester resin and then ground and polished (using automatic polisher Struers - Jean Wirtz TF250* machine) using SiC papers and diamond slurries. As mentioned above, the polishing method is very important in imaging

these structures. The polishing procedure used here required significantly longer times (more than 10×) for each polishing step compared to the procedures suggested by the manufacturer of the polisher. The reason for this was that damage in the forms of pull outs was extensive and therefore it was necessary to remove thicker layer than usual in each step. Polishing was controlled by means of an optical microscope of regular intervals and each sample required different times in each step, depending on its resistance to forming pull-outs. Therefore, it is impossible to specify a single procedure for all of these samples.

Polished cross sections of selected samples were studied using SEM (CamScan*, Great Britain). Structures are presented in BE (back-scattered electrons) mode at magnifications 1000× and 1500×. Resulting gray scale pictures were further enhanced on a PC computer.

Small-angle neutrons scattering experiments were carried out on the 8 m SANS instrument* at the NIST Cold Neutron Research Facility at the National Institute of Standards and Technology in Gaithersburg, MD, USA.

RESULTS

Results of the SEM imaging are presented in figures 2 and 3. The MIP results are summarized in the table 2.

Table 2. Results of the MIP measurements. Twice the estimated standard deviation (2σ) is shown in parentheses.

material spray process	alumina (%) (1)	zirconia (YSZ) (%) (1)
APS (gas-stabilized PS)	15	15
WSP® (water-stabilized PS)	8	12

Table 3. Results of the SANS analysis.

material spray process	**alumina** surface ratio** total voids surface area	**zirconia (YSZ)** surface ratio** total voids surface area
APS (gas-stabilized PS)	50 : 50 1.47 10^4 cm^2 cm^{-3}	15 : 85 2.62 $10^4 cm^2 cm^{-3}$
WSP® (water-stabilized PS)	85 : 15 1.73 $10^4 cm^2$ cm^{-3}	20 : 80 2.60 $10^4 cm^2 cm^{-3}$

** XX : YY represents fractions of surface areas in CRACKS : : (interlamellar) PORES

DISCUSSION

Figures 2 and 3 show similar lamellar microstructures characteristic for plasma sprayed deposits. While all of these have characteristics in common, one can determine the important way in which the plasma-sprayed deposits differ as a function of spray method and chemistry.

There are observable variations in the microstructures of alumina deposits (figure 2*a* and *b*) deposited by different spraying techniques. GSP alumina has finer structure with more interlamellar pores and thinner splats. The WSP® has thicker splats and more than GSP deposits a good contact in between them. There are, however, more vertical cracks in the WSP® deposits and possibly also less of rounded pores.

YSZ deposits (figure 3*a* and *b*) showed much more similar microstructures with large number of pores and cracks. There seem to be no visible dependence on the spray technique for this material.

More distinct differences can be observed between alumina and YSZ deposits (figures 2 and 3). YSZ deposits have more observable lamellar microstructure with more visible interlamellar pores, suggesting worse contact between the lamellae.

It is important to note, that quantitative analysis of these micrographs is complicated by the fact, that many smaller voids are difficult to distinguish. These may be therefore neglected which may distort the results. Each micrograph shows also some damage (pull outs) related to sample preparation.

The porosity volumes measured by MIP vary from 5 % to 15 %, which is usual range of porosities of these materials with WSP® deposits having lower porosities for each chemistry than GSP deposits.

The SANS results are presented in the figures 4 to 7. These show 3-d distributions of apparent Porod surface areas. Apparent Porod surface area distribution represents distribution of measured Porod surfaces in whole 3-d (4π). The simplest way to imagine what these apparent Porod surfaces mean is to imagine observing the sample from center within. Such observer would in any particular direction observe just measured apparent Porod surface area. Important feature of the apparent Porod surfaces is, that if these are known over whole 3-d, they can be integrated and the quantitative information about the real surfaces within the sample can be recovered. Each distribution can be decomposed into two spheroids as in figure 7. These two spheroids of apparent Porod surface area distribution can be quantitatively evaluated and the fractions of surface areas within each system are presented in the table 3. This table shows a significant difference between the microstructures, which cannot be seen from MIP and can only be observed with difficulties in microscopy. There is a variation in the proportions of

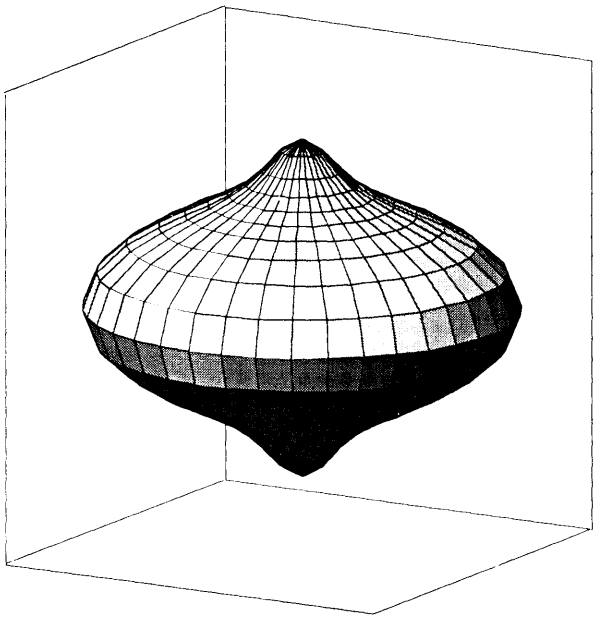

Figure 4. Apparent Porod surface area distribution of WSP® deposited alumina. Apparent Porod surface area can be defined as Porod surface area which would be viewed in any particular direction by observer standing in the center of the sample. Knowledge of this apparent surface area in all directions (over 4π) allows calculation of the quantitative specific surface area in the sample and, if more surface systems can be distinguished, in the surface systems separately.

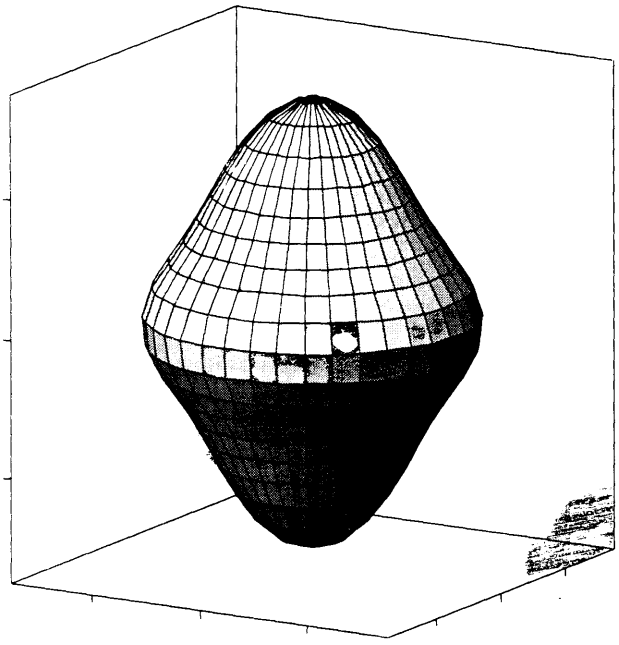

Figure 5. Apparent Porod surface area distribution of GSP deposited alumina. For explanation of apparent Porod surface area see caption of figure 4.

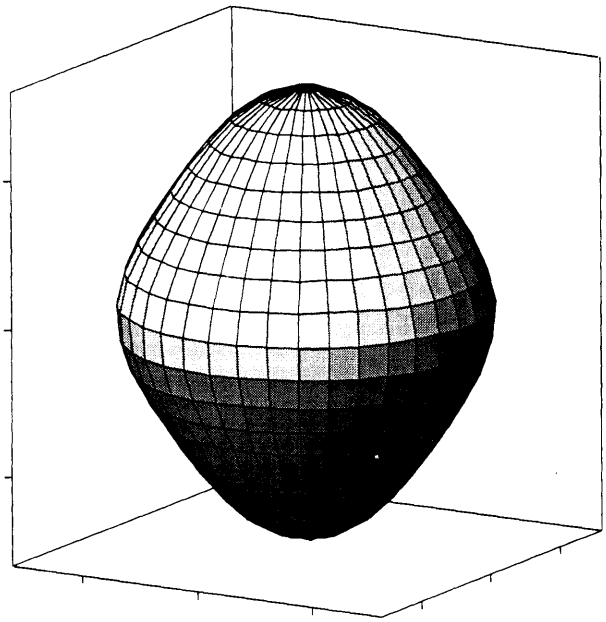

Figure 6. Apparent Porod surface area distribution of GSP deposited zirconia. For explanation of apparent Porod surface area see caption of figure 4.

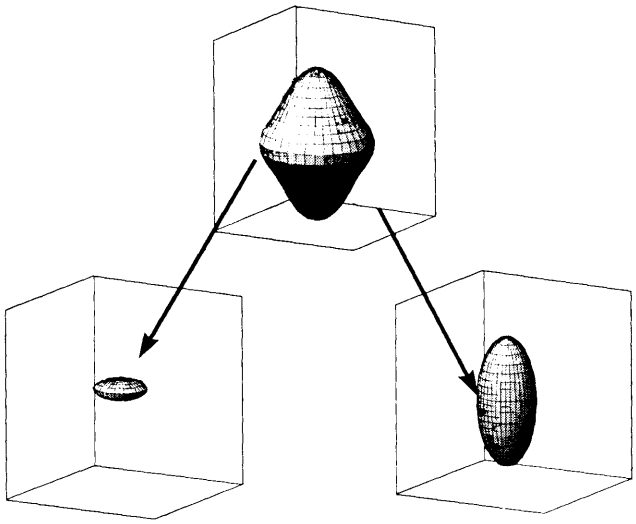

Figure 7. The apparent Porod surface area distribution of GSP deposited alumina separated into two separate void surface areas. Left (prolated ellipsoid) representing intralamellar cracks and right (elongated ellipsoid) representing intralamellar pores. For explanation of apparent Porod surface area see caption of figure 4.

the surface area found in the interlamellar pores and cracks surfaces. The SANS characterization is not complete since the volume in each system and the sizes of these voids are not available, but it gives a significantly better description of the structure than MIP and it is more quantitative and statistically representative than image analysis. As mentioned above the rounded pores are not seen separately in this method and their assessment using another SANS techniques will be described in a future publication [20].

The SANS results indicate that the GSP and WSP® alumina microstructures are significantly different. Similar differences in the microstructures were found in the SEM (figures 2 and 3). However, here the result is quantitative and quite striking. The interlamellar contact in WSP® alumina was found to be significantly better than in the GSP alumina. Since the cooling stresses formed in each splat during cooling after impact cannot be relaxed by sliding, the splats crack. This is the likely reason for significantly higher crack surface areas.

Zirconia has greater toughness than alumina - and the crack surfaces formed about 15 % to 20 % of the total void surface area. The crack surfaces within the alumina deposits, on the other hand, represented at least 50 % or more of the total. For WSP® alumina (which is a process with higher temperatures) the cracks represented up to 80 %, showing, that they are dominant features in these materials.

CONCLUSION

Plasma spraying produces a wide range of microstructures. These microstructures may contain varying amounts of cracks and interlamellar pores, each with different orientational distribution. The SANS technique of Porod scattering is an illuminating technique which allows separate and quantitative characterization of these void systems.

Characterization techniques such as MIP and image analysis have limitations in addressing the anisotropy of the voids system in these deposits and therefore need to be complemented with SANS measurements. Together this type of characterization offers a new understanding of the void structure. This enables building a new understanding of the relationships between the structure and properties of these deposits.

* Names of commercial products are given for completeness and should not be considered an endorsement by NIST.

Acknowledgement

Authors would like to thank Dr. R. Gansert for supplying them with CaSZ WSP® sample. Authors would also like to gratefully acknowledge support by grants by the NSF N° INT9317415 as well by the Grant Agency of the Academy of Sciences of the Czech Republic N° AVK 1010601.

We acknowledge the support of the National Institute of Standards and Technology, U. S. Department of Commerce, in providing the neutron research facilities used in this work.

References

1. Herman H.: Scientific American *259*, 112 (1988).
2. Kubel E. J. Jr.: Adv. Mater. And Process *132*, 69 (1987).
3. Lugscheider E., Eschnauer H., Muller U., Weber Th.: Powder Metal. Int. *23*, 30 (1991).
4. Ilavsky J.: Studies of Plasma Sprayed Alumina, Ph.D. Dissertation, SUNY at Stony Brook, NY 1994.
5. Thompson V. S. and Whittemore O. J., Jr.: Am. Ceram. Soc. Bull. *47*, 637 (1968).
6. Grunling H. W., Manasmann W.: J. de Physique IV *3*, 903 (1993).
7. McPherson R.: Thin Solid Films *83*, 297 (1981).
8. McPherson R., Shafer B. V.: Thin Solid Films *97*, 201 (1982).
9. Ilavsky J., Allen A. J., Long G. G., Krueger S., Herman H., Berndt C. C., Goland A. N. in: *Thermal Spraying - Current Status and Future Trends*, edited by A. Ohmori, p.483 - 488, High Temperature Society of Japan, Osaka, Japan 1995.
10. Pekshev P. Yu., Safiullin V. A. in: *High-Temperature Dust Laden Jets in Plasma Technology*, edited by O. P. Solonenko and A. I. Fedorcenko, p. 437 - 462, VSP BV, Zeist, The Netherlands 1990.
11. Safai S., Herman H. in: *Advances in Surface Coating technology*, paper 5, Welding Inst., London 1978.
12. Ilavsky J., Herman H., Berndt C. C., Goland A. N., Long G. G., Krueger S., Allen A. J. in: *1994 Thermal Spray Industrial Applications*, edited by C.C. Berndt and S. Sampath, p. 709 -714 ASM Int., Materials Park, OH 1994.
13. Ilavsky J., Allen A.J., Long G.G., Krueger S., Berndt C.C., Herman H.: J. Am. Ceram. Soc. *80* , 733 (1997).
14. Krueger S., Long G.G., Page R.A.: Acta Cryst. *A47*, 282 (1991).
15. Long G. G., Krueger S., Gerhardt R. A., Page R. A.: J. Mater. Res. *6* , 2706 (1991).
16. Porod G. in: *Small-angle X-ray Scattering*, edited by O. Galtter and O. Kratky, p.17 - 51, Academy Press, London 1982.
17. Kostorz G. in: *Treatise on Materials Science and Technology*, edited by G. Kostorz, Vol. 15, p. 227-290, Academic Press, NY 1979.
18. Weertman J.R. in: *Nondestructive Evaluation: Microstructure Characterization and Reliability Strategies*, p. 147-168, American Inst. of Mining, Metallurgical and Petroleum Engineers, NY 1981.
19. Hamzeh F. M., Bragg R. H.: J. Appl. Physics *45*, 3189 (1974).

20. Ilavsky J., Long G. G., Allen A. J., paper under preparation.
21. Fowler D. B., Riggs W., Russ J. C. in: *Thermal Spray: Research and applications, Thermal Spray Research and Applications*, edited by T. Bernecki, p. 303-313, ASM Int., Materials Park, OH 1990.
22. Glancy S. D. in: Structure (Struers Jour. of Materialography) *29*, 12 (1996).
23. Karthikeyan J. in: *Thermal Spraying - Current Status and Future Trends*, edited by A. Ohmori, p. 927-932, High Temp. Soc. of Japan, Osaka, Japan 1995.
24. Ilavsky J., Berndt C.C., Karthikeyan J.: J. of Mater. Sci. *32*, 3925 (1997).
25. Gregg S. J. and Sing K. S .W. in: *Adsorption, Surface Area and Porosity*, p. 173-195, Academic Press, London (1982).
26. Lee H. H. D.: J. Am. Ceram. Soc. *73*, 2309 (1990).
27. *Standard test method for measurement of density of glass by buoyancy*, ASTM C693-84, ASTM, Philadelphia, PA, USA, 1985.

Submitted in English by the authors.

POUŽITÍ MALOÚHLOVÉHO ROZPTYLU NEUTRONŮ NA CHARAKTERIZACI ANIZOTROPNÍCH STRUKTUR VZNIKLÝCH PLAZMOVÝM NANÁŠENÍM

JAN ILAVSKY*, **, GABRIFLLE G. LONG**, ANDREW J. ALLEN**, HERBERT HERMAN***, CHRISTOPHER C. BERNDT***

**Ústav fyziky plazmatu, Akademie věd České republiky, Za Slovankou 3, 182 00 Praha*

***National Institute of Standards and Technology, Gaithersburg, MD 20899, USA*

****State University of New York at Stony Brook, Stony Brook, NY 11973, USA*

Plazmově nanášené keramické vrstvy mají komplikovanou mikrostrukturu, ve které je dominantní anizotropní systém pórů. Tyto póry lze rozdělit na dva anizotropní druhy: mezilamelární póry, přednostně orientované paralelně s podložkou a trhlinky uvnitř jednotlivých ztuhlých kapek (anglicky splat), orientované přibližně kolmo k podložce. Oběma těmto typům lze přiřadit přibližně diskovitý tvar a při relativně malém objemu mohou mít značný povrch. Třetím významným typem pórů, který je pozorován v těchto materiálech jsou duté útvary přibližně kulového tvaru. Tyto nejsou anizotropní a přestože mohou reprezentovat značnou část objemu pórovitosti mají relativně malý povrch.

Charakterizace takto komplikovaných anizotropních struktur je obtížná. Vtlačovací metody, které se používaji ke stanovení pórovitosti, např. rtuťová pórometrie, nevystihují anizotropii. Použití obrazové analýzy řezů vzorků je rovněž ztíženo, neboť plazmově nanesené vrstvy jsou velmi křehké a výbrusy běžně obsahují řadu artefaktů (vypadané částice), které zkreslují skutečnou strukturu pórů. Navíc je vyhodnocení řezů komplikované různou anizotropií typů pórů, která vyžaduje náročnou prostorovou rekonstrukci při více řezech.

Maloúhlový rozptyl neutronů (SANS) je v této oblasti nová technika, která charakterizuje anizotropní systém pórů pomocí trojrozměrného (3-D) anizotropního rozdělení průmětů jejich povrchů – rozdělení povrchu podle Poroda. Tato technika zkoumá najednou značný objem vzorku a výsledky představují statisticky zprůměrovanou informaci získanou na velkém objemu (10 až 50 mm^3).

Článek prezentuje použitou techniku maloúhlového rozptylu (SANS) a porovnává výsledky získané na vzorcích ze dvou keramických materiálů (ZrO_2 stabilizovaného 8 hmot.% Y_2O_3 (PSZ) a Al_2O_3) nanášených dvěma obdobnými plazmovými technologiemi – plazmatem, stabilizovaným plynem (GSP) a vodou (WSP®). Výsledky ze SANS jsou porovnány s výsledky získanými rtuťovou pórometrií (tabulka 2) a obrazovou analýzou na řádkovacím elektronovém mikroskopu (obrázky 2 a 3).

Výsledky maloúhlového rozptylu jsou v obrázcích 4 až 7. Obrázky 4 až 6 ukazují, že sledované vzorky mají velmi rozdílná rozdělení povrchu podle Poroda a tedy i rozdílné struktůry pórů. Obrázek 7 demonstruje, jak jsou jednotlivé systémy pórů, díky rozdílné anizotropii, reprezentovány různými elipsoidy v 3-D rozdělení povrchu podle Poroda. Rozdílná velikost a tvar těchto elipsoidů odráží celkový povrch a anizotropii každého systému pórů zvlášť. Integrováním separovaných elipsoidů lze získat kvantitativní informaci o celkovém měrném povrchu každého pozorovaného systému pórů zvlášť. Tyto výsledky jsou kalibrovány pomocí externích standardů. Porovnáním tvaru (excentricity) elipsoidu před a po dalším zpracování vzorku (např. žíhání) lze získat představu o změnách tvarů nebo orientace pórů.

Tabulka 2 a obrázky 2 a 3 ukazují, jaké jsou rozdíly mezi sledovanými vrstvami získané standardními měřícími technikami. Rtuťová pórometrie stanovila významné rozdíly mezi objemy pórovitosti u jednotlivých vzorků (tabulka 2). Obrazová analýza (obrázky 2 a 3) naznačuje obdobné rozdíly v objemu pórovitosti a navíc napovídá, že mezi strukturami jsou rozdíly v zastoupení jednotlivých druhů pórů. Kvantifikace tohoto zastoupení je však obtížná. V tabulce 3 jsou uvedeny výsledky získané metodou SANS, které ukazují na mnohem zásadnější rozdíly v charakteru pórovitosti: materiály i vrstvy nanesené různými technikami se liší jak celkovou plochou, tak různým poměrným zastoupením obou anizotropních systémů pórů. Vrstvy Al_2O_3 obsahují výrazně více trhlin uvnitř splatů, zvláště po nanesení pomocí vodou stabilizovaného plazmatu, než vzorky PSZ. Současně mají vrstvy PSZ větší celkový měrný povrch pórů. Tento výsledek dokládá, že vlastnosti těchto vrstev se mohou lišit jak velikostí tak i svojí anizotropií, například tepelná vodivost či mechanické vlastnosti.

Výsledky této studie ukazují, že standardní metody stanovení pórovitosti v těchto anizotropních materiálech nejsou dostatečné a že je třeba využívat možností nových metod. Metoda maloúhlového rozptylu je jednou z těchto technik a přináší nový náhled na strukturu, kterou je možné použít při optimalizaci vlastností vrstev pro různé aplikace.